MEASUREMENTS AND MODELING OF RADIO PROPAGATION IN LARGE OFFICES WITH LOW METALLIC PARTITIONS

Kung-Min Ju and Jenn-Hwan Tarng
Department of Communication Engineering
National Chiao-Tung University
Hsin-Chu, Taiwan, Republic of China

KEY TERMS

Indoor radio propagation, knife-edge diffraction, low partitions

ABSTRACT

A theoretical model is developed to predict the propagation loss of UHF radio waves in large modern offices with low metallic partitions. It is found that in addition to free-space propagation loss, the shadowing loss due to the blockage by the low partitions in the out-of-sight situation becomes the dominant one. The shadowing loss can be efficiently formulated by using the theory of single or double knife-edge diffraction. The model has been verified by an experiment conducted at 905 MHz, 1.75 GHz, and 2.44 GHz in large offices. The model shows reasonable accuracy. © *1996 John Wiley & Sons, Inc.*

1. INTRODUCTION

Radio propagation in the UHF band has been proposed as a basis for radio local area networks (RLANs) and personal communications services (PCS) [1, 2]. The ultimate goal of PCS is to provide instant communications between individuals located anywhere in the world, at any time. In particular, when providing service in densely populated buildings, which would have traffic many times greater than that of vehicular mobile radio systems, a floor or even a room may represent a cell [3]. Hence, there is a need to establish a prediction model of propagation losses that takes into account various configurations and building materials. An accurate prediction model can make planning and installation of these systems as easy and cheap as possible. In addition to the great deal of experimental data and the many empirically based models that have been reported, theoretical models that use the ray-tracing method [4, 5] or that involve the waveguide model [6] have been proposed to predict propagation losses on the same floor of office buildings. The major goal of this research is to investigate the effects of the geometrical structure on radio propagation in building rooms and corridors. The effects of objects (low partitions, desks, chairs, cabinets, and furnishings, etc.) inside the room on radio propagation have not been investigated in detail because of practical complexity and difficulty [4]. Here, a theoretical model is developed and can easily predict the propagation loss in a large office with low metallic partitions, which are common geometrical features in modern offices. The shadowing loss due to the blockage by the low partitions is formulated by the theory of single or double knife-edge diffraction [7, 8]. Experiments with radio waves at 905-MHz, 1.75-GHz, and 2.44-GHz radio frequencies on fixed indoor links in two different office buildings are conducted to verify the accuracy of the model.

The rest of the article is organized as follows. The measurement equipment, environments, and results are described in Section 2. In Section 3, the theoretical model used to predict field strength is developed, and the computed results are compared with the measured ones. Conclusions are drawn in the last section.

2. MEASUREMENT EQUIPMENT, ENVIRONMENTS, AND RESULTS

The field strength was measured in two different large offices, No. 1 and No. 2. Detailed parameters of the four experiments are given in Table 1. All measurements were made with the transmitting antenna held stationary, while the receiving antenna was placed in different locations in the same room. The layout of office No. 1 is shown in Figure 1, which is located on the second floor of a three-story reinforced-concrete building. The front and back walls are made of concrete, and the right and left side walls are constructed of a 4-m-high aluminum window frame, extending from ground to ceiling. Besides the low metallic partitions, there are wooden desks, chairs, filing cabinets, and concrete pillars inside the office. The layout of office No. 2 is illustrated in Figure 2. It is situated on the third floor of another building. In this room, only the left side wall is constructed of an aluminum window frame; the rest of the walls are made of concrete. Furnishings similar to those in office No. 1 were also found in office No. 2. The height of the partitions is the same; 1.35 m above the floor.

Figure 3 is a block diagram of the measurement system. Half-wavelength dipole antennas with 2.15 dB of gain relative to the isotropic antenna were used throughout the 1.75-GHz and 2.44-GHz measurements in the transmitter and receiver. Two types of antennas were used in 905-MHz measurement. The receiving antenna is a quarter-wavelength monopole antenna, and the transmitting antenna is a half-wavelength dipole antenna. In the 1.75-GHz and 2.44-GHz cases, a frequency converter is added right before the receiver to downshift the receiving frequency.

Because all of the objects inside the office can serve as scatterers or reflectors to the radio wave, they cause the received signal to exhibit strong variations as the receiving antenna is moved over a short distance on the order of 0.5 wavelength. In our experiment, the section average of field strength at each measuring point is obtained by averaging over nine measured subpoints within a circle of radius equal to 0.75 wavelength. The data of each subpoint are time-averaged signals over a suitable time period with a 10-Hz data sampling rate.

In Figure 4, the measured and free-space propagation losses (in decibels, with respect to 1-m free-space propagation loss) of Experiment I are illustrated by the solid and dashed lines, respectively. The former line is fitted by the method of least-square regression from the measured data with attenuation slopes equal to -33.5 (dB/decade). For Experiments II–IV, the attenuation slopes are equal to -38.5 (dB/decade), -37.3 (dB/decade), and -37.0 (dB/decade), respectively. It is observed that excess loss of four measurements ranges from 6 to 24 dB, which may be due to the shading of the low partitions. This will be verified in the next section.

3. THEORETICAL MODELS

In our model, waves reflected from rough ceilings, aluminum window frames, or furnishings are neglected. Because the low partitions are attached to the ground, the ground reflections can be ignored. Therefore, it is believed that the excess path loss is mainly due to shading losses from the low metallic partitions. Modeling the radio waves diffracted by the low partitions is our major concern. The theories of single and double knife-edge diffractions are used to formulate the diffraction losses of the low partitions.

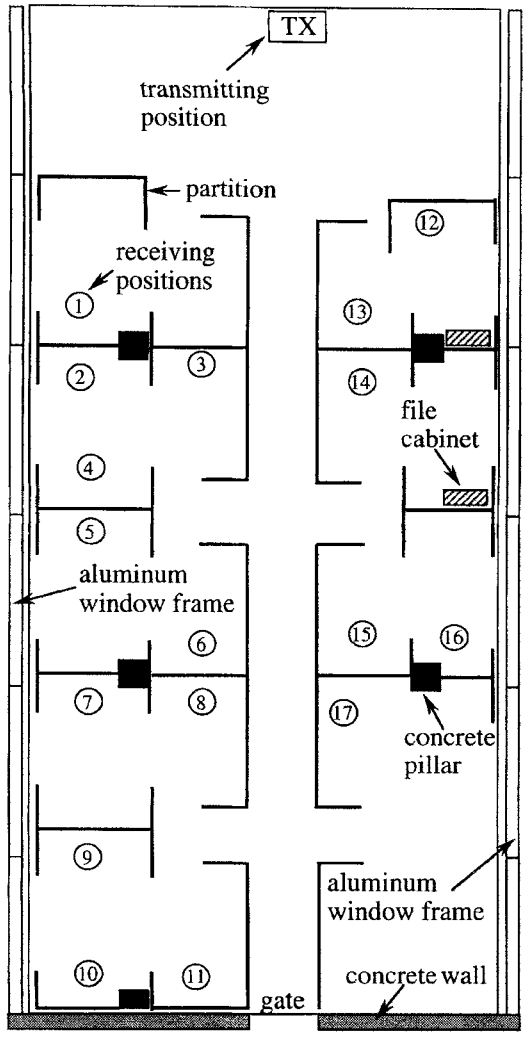

Figure 1 The layout of office No. 1 (30 m × 10 m × 4 m), in which Experiment I is carried out

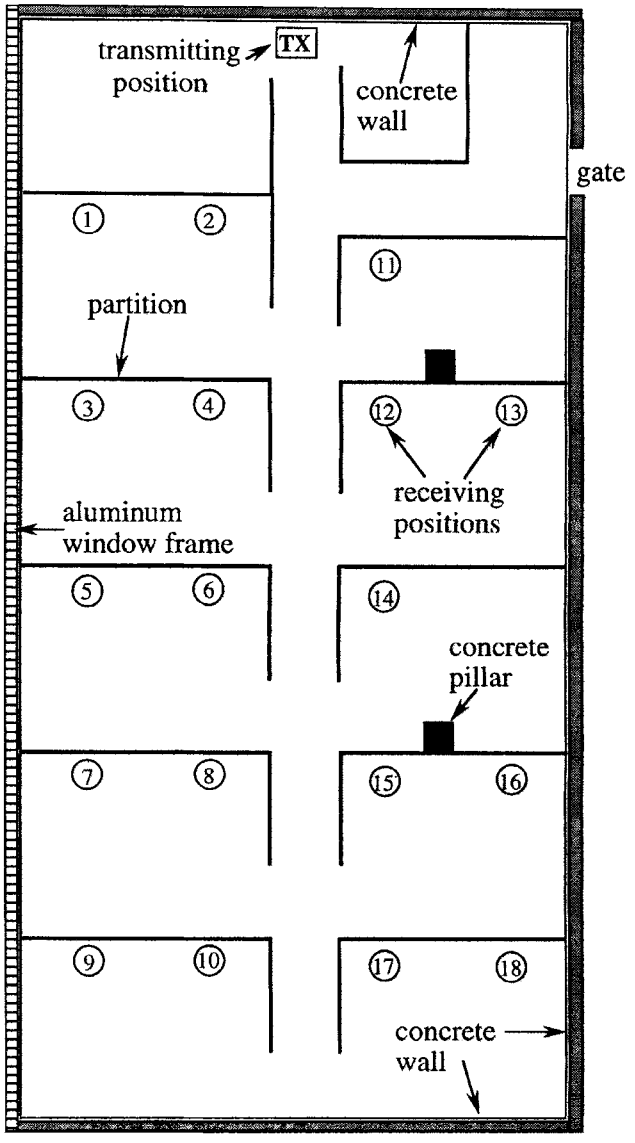

Figure 2 The layout of office No. 2 (20 m × 10 m × 3 m), in which Experiments II–IV are carried out

A. Single Knife-Edge Diffraction. Compared with the propagation wavelength, the thickness of the low partition is thin enough that it can be neglected. Hence the theory of single knife-edge diffraction is employed to evaluate the diffraction loss of one partition. According to the theory in Reference [7] and the geometry given in Figure 5, the electric field after diffraction is given by

$$E_d = E_f F(v), \tag{1}$$

where E_f is the free-space electric field, and is equal to

$$E_f = E_0 \frac{e^{-jkd}}{d}, \tag{2}$$

with $d = d_1 + d_2$ representing the distance between the transmitter and the receiver. Here, E_0 and k represent the

TABLE 1 Experimental Parameters

	Experiment			
	I	II	III	IV
Site	Office No. 1	Office No. 2	Office No. 2	Office No. 2
Frequency (MHz)	905	905	1750	2440
P_t (dBm)	0	10	10	10
Polarization	vertical	vertical	vertical	vertical
h_t (m)	1.8	1.8	2.5	2.5
h_r (m)	0.85	1.0	1.0	1.0
Test points	17	10	15	17

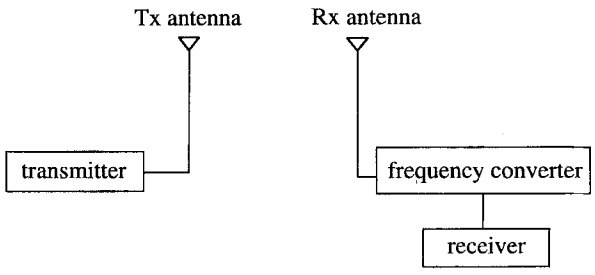

transmitter	signal generator (Marconi 2031)
receiver	test receiver (Anritsu ML524B)
freq. converter	(Anritsu MH669B)
Tx antenna	0.5λ dipole (Anritsu)
Rx antenna	0.5λ dipole (Anritsu) or 0.25λ monopole

Figure 3 Measuring system block diagram and equipment description

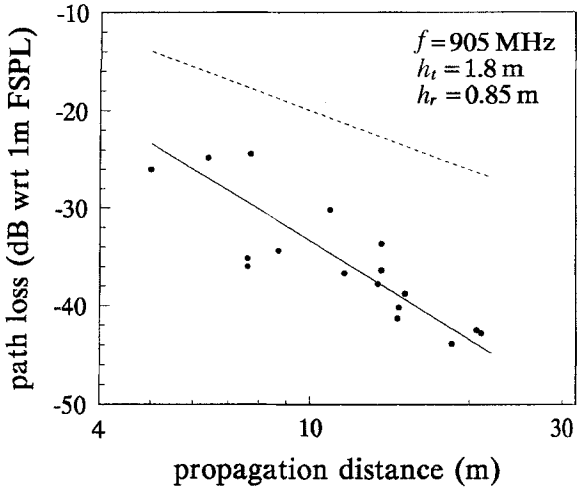

Figure 4 The measured and free-space propagation losses (in decibels with respect to 1-m free-space propagation loss) of Experiment I

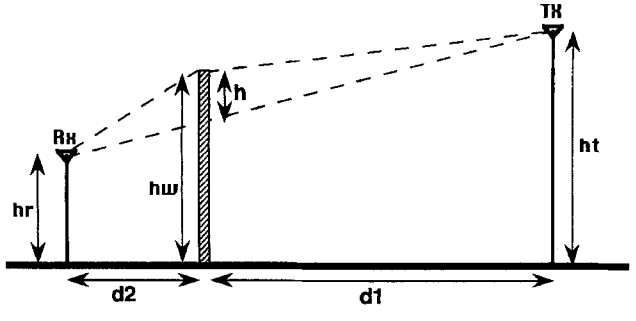

Figure 5 Geometry for single knife-edge diffraction

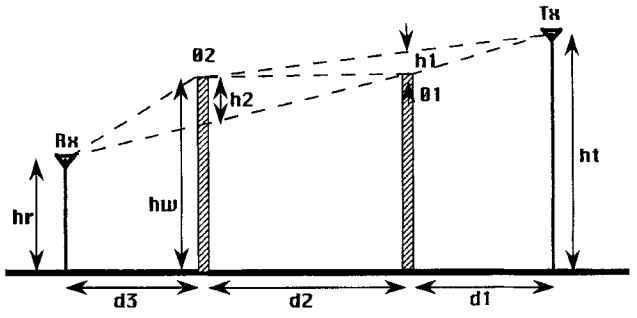

Figure 6 The Epstein-Peterson diffraction model for double knife-edge diffraction

relative source amplitude and free-space wave number, respectively. $F(v)$ is the diffraction coefficient given by

$$F(v) = \frac{1+j}{2}\int_v^\infty e^{-j(\pi/2)t^2}\,dt, \tag{3}$$

where v is the Fresnel diffraction parameter given by

$$v = h\left[\frac{2(d_1+d_2)}{\lambda d_1 d_2}\right]^{1/2},$$

with

$$h = (h_w - h_r) - (h_t - h_r)\frac{d_2}{d_1+d_2}.$$

The received field strength $E_r = 20\log_{10}|E_d|$ is given by

$$E_r = 20\log_{10}|E_f| + 20\log_{10}|F(v)|. \tag{4}$$

B. Double Knife-Edge Diffraction. Because there is more than one low partition blocking the direct path for some measuring points, the multiple knife-edge diffraction model is employed to give a more accurate prediction. To simplify the computation, only double knife-edge diffraction is considered. Here, we use the Epstein-Peterson diffraction-loss method [8], which has been proven to be an accurate model, to compare with the rigorous analytical solution [9], to compute the double knife-edge diffraction loss due to two separated partitions. The Epstein-Peterson diffraction is an extension of the single knife-edge diffraction, and its construction is shown in Figure 6. The received field strength after double knife-edge diffraction is evaluated as the sum of two single knife-edge diffractions whose geometries are given in Figure 6 for paths T-01-02 and 01-02-R. It can be evaluated by using Eqs. (1) and (4) with $d = d_1 + d_2 + d_3$ and $F(v) = F(v_1)F(v_2)$.

From Figure 6,

$$v_1 = h_1\left[\frac{2(d_1+d_2)}{\lambda d_1 d_2}\right]^{1/2}$$

and

$$v_2 = h_2\left[\frac{2(d_2+d_3)}{\lambda d_2 d_3}\right]^{1/2}.$$

Here,

$$h_1 = (h_w - h_t)\frac{d_2}{d_1 + d_2}$$

and

$$h_2 = (h_w - h_r)\frac{d_2}{d_2 + d_3}.$$

It is noted that all the partitions are the same height, and v_1 and v_2 can be positive or negative.

C. Comparison between Measured and Predicted Field Strengths. In Figures 7–10, the measured and predicted field strengths are illustrated as a function of propagation distance for Experiments I–IV, respectively. It is noted that the difference between the predicted and measured field strengths in Experiment IV is larger than in other experiments. This is because the waves scattered by rough ceiling surfaces, window frames, or furnishings will tend toward a specular reflection as the radio frequency is increased. Therefore, the effects from any object inside the offices for indoor radio propagation at the higher frequency band must be taken into account. In order to verify the prediction accuracy of our model, the average of the error and its standard deviation are calculated for each experiment. The averaged errors are −2.5 dB, 0.8 dB, 0 dB, and 0.6 dB, and their standard deviations are 2.4 dB, 2.9 dB, 2.9 dB, and 4.9 dB, for experiments I–IV, respectively. The overall averaged error is equal to = −0.4 dB. All of the values shown above are better than those in Reference [4].

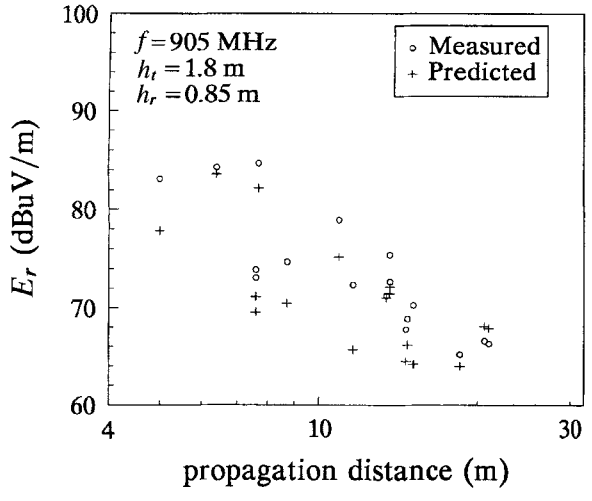

Figure 7 The measured and predicted field strengths of Experiment I

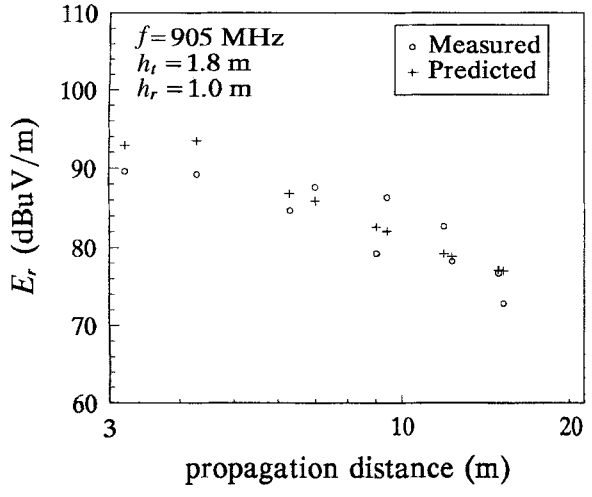

Figure 8 The measured and predicted field strengths of Experiment II

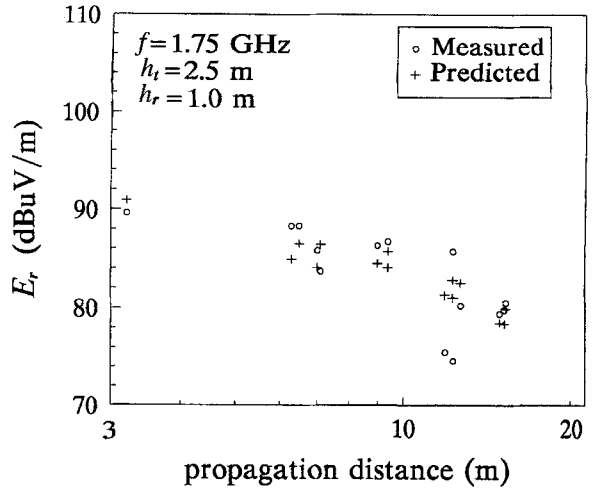

Figure 9 The measured and predicted field strengths of Experiment III

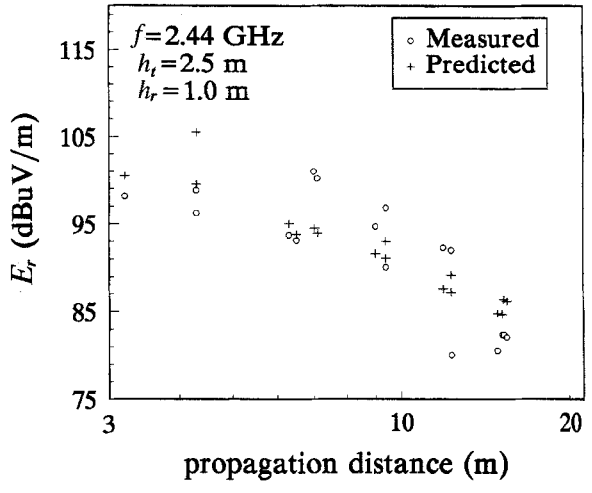

Figure 10 The measured and predicted field strengths of Experiment IV

4. CONCLUSION

In this study, models of radio propagation in large offices with low metallic partitions are developed based on the theory of single and double knife-edge diffraction. To verify the prediction accuracy of the models, propagation experiments at 905-MHz, 1.75-GHz and 2.44-GHz radio frequencies on fixed indoor radio links in two different offices are conducted. It is found that the accuracy of our models compares quite well with the mean-square error and the standard deviation of error of the field strengths, all being less than 5 dB. This shows that in addition to the free-space

propagation loss, the diffraction loss due to multiple low partitions is the major mechanism governing the excess loss in out-of-sight situations. Reflections from the plasterboard walls, aluminum window frames, and the ground can be neglected.

ACKNOWLEDGMENT

This research is supported by the National Science Council of Taiwan under Grant No. NSC 84-2221-E-009-017.

REFERENCES

1. M. Marcus, "Regulatory Policy Considerations for Radio Local Area Networks," *IEEE Commun. Mag.*, Vol. 25, No. 7, 1987, pp. 95–99.
2. H. Hashemi, "The Indoor Radio Propagation Channel," *Proc. IEEE,* Vol. 81, No. 7, 1993, pp. 943–968.
3. D. Molkdar, "Review on Radio Propagation into and within Buildings," *IEE Proc. Pt. H,* Vol. 183, No. 1, 1991, pp. 61–73.
4. W. Honcharenko, H. L. Bertoni, J. L. Dailing, J. Qian, and H. D. Yee, "Mechanisms Governing UHF Propagation on Single Floors in Modern Office Buildings," *IEEE Trans. Veh. Technol.,* Vol. VT-41, No. 4, 1992, pp. 496–504.
5. S. Y. Seidel and T. S. Rappaport, "Site-Specific Propagation Prediction for Wireless In-Building Personal Communication System Design," *IEEE Trans. Veh. Technol.,* Vol. VT-43, No. 4, 1994, pp. 879–892.
6. G. M. Whitman, K-S Kim, and E. Niver, "A Theoretical Model for Radio Signal Attenuation Inside Buildings," *IEEE Trans. Veh. Technol.,* Vol. VT-44, No. 3, 1995, pp. 621–629.
7. E. C. Jordan and K. G. Balmain, *Electromagnetic Waves and Radiating Systems,* Prentice-Hall, New York, 1968.
8. J. Epstein and D. W. Peterson, "An Experimental Study of Wave Propagation at 850 Mc," *Proc. IRE41,* No. 5, 1953, pp. 595–611.
9. R. E. Wilkerson, "Approximation of the Double Knife-Edge Attenuation Coefficient," *Radio Sci.,* Vol. 1, No. 12, 1966, pp. 1439–1443.

Received 1-31-96

Microwave and Optical Technology Letters, 12/3, 172–176

CCC 0895-2477/96

EXACT SOLUTION OF NONLINEAR SURFACE WAVES GUIDED BY A NON-KERR-LIKE, POWER-LAW-DEPENDENT MEDIUM

M. M. Shabat
Physics Department
Islamic University of Gaza
P.O. Box 108
Gaza, Gaza Strip,
Palestinian Authority

A. D. Boardman
Physics Department
Salford University
Manchester, M5 4WT, United Kingdom

R. Reinisch and E. Pic
Laboratorie d'Electromagnétisme, Microonodes et Optoélectronique
URA CNRS 833
ENSERG
23 ave des Martyrs
BP 257
38016 Grenoble Cedex, France

KEY TERMS

Waveguide, nonlinear optics, surface waves

ABSTRACT

An exact analytical dispersion relation describing the propagation of TE s-polarized electromagnetic surface waves along the interface of a non-Kerr-like, nonquadratic, power-law-dependent cover and a linear dielectric substrate has been derived. The power flow carried versus the wave index, and the field distributions have also been computed. © 1996 John Wiley & Sons, Inc.

INTRODUCTION

Systems involving nonlinear dielectric media and their interaction with light waves are potentially useful in various important practical applications in nonlinear optics, signal and data processing, and optical computers [1–8]. Most published articles concentrate on the behavior of nonlinear surfaces, and on guided waves in nonlinear Kerr-like media, where the refractive index depends upon the quadratic optical field intensity, and exact solutions [1–8] have been obtained for TE s-polarized nonlinear waves. There are no analytical solutions reported about TE s-polarized waves guided by non-Kerr-like nonquadratic, power-law-dependent media, where the permittivity of the medium can be considered a function of the absolute value of the electric field and can be written [8–13] as $\epsilon^{nk} = \epsilon_2 + \alpha|E|$. Langbein and co-workers [8, 9] studied this problem by using the first integral approach of the nonlinear wave equation, which is subsequently used in satisfying the boundary conditions. The above approach is based on numerical techniques and was used [11–13] in computing the field distributions and the power-flow configurations. In this article we derive a new exact analytical dispersion relation of electromagnetic waves that propagate along the boundary of a non-Kerr-like, nonquadratic, power-law-dependent cover and a linear dielectric substrate. Both of the field distributions versus the position and the power flow versus the wave index have also been computed. This approach can easily be used in modeling some waveguides, which could be used in optoelectronics and integrated-circuit technology.

STRUCTURE OF THE PROBLEM AND DISPERSION RELATIONS

The structure consists of a linear dielectric substrate, of dielectric permittivity ϵ_1, occupying the half space $z < 0$ in Region I, and a non-Kerr-like, non-quadratic, power-law-dependent cover, where the permittivity can be considered as a function of the absolute value of the optical electric field [6, 7] as $\epsilon^{nk} = \epsilon_2 + \alpha|E|$, occupying the half space $z > 0$, in Region II. We consider TE s-polarized waves that propagate in the x direction. It is therefore convenient to write the only nonvanishing components of E and H in the form

$$H_{x,z}(x, z, t) = H_{x,z}(z)e^{i(kx-\omega t)},$$
$$E_y(x, z, t) = E_y(z)e^{i(kx-\omega t)}, \quad (1)$$

where k is the surface wave number, and ω is the angular frequency.

For the two semiinfinite bounding media, the fields must decay to zero as $z \to \pm\infty$, so the fields $E_y(z)$, $H_x(z)$, and $H_z(z)$ are completely real, as is the case for nonlinear surface waves guided by a Kerr-like medium [2]. We start our calculation from the Maxwell equations,

$$\nabla \times \underline{E} = i\omega\mu_0\underline{H}, \quad (2a)$$
$$\nabla \times \underline{H} = -i\omega\epsilon_0\epsilon\underline{E}, \quad (2b)$$